JOURNAL OF SOLID STATE CHEMISTRY **136,** 263–268 (1998)
ARTICLE NO. SC977699

EPR Study of Mo^V in the Tetragonal and Monoclinic Phases of Zirconia

Dante Cordischi,[1] Manlio Occhiuzzi, and Roberto Dragone

Centro SACSO (CNR), Dipartimento di Chimica, Università La Sapienza, Rome, Italy

Received June 2, 1997; in revised form November 7, 1997; accepted November 10, 1997

MoO_x/ZrO_2 (^{95}Mo-enriched or not) samples were prepared by adsorption or coprecipitation and were subsequently heated in air or oxygen at 773 or 1073 K. Depending on the heating temperature and the Mo content, clustered Mo^V species (Mo^V_{clust}) and isolated Mo^V species in tetragonal (Mo^V_{tetr}) and/or monoclinic (Mo^V_{mon}) phases were formed. Mo^V species were detected by EPR only at low temperature (77 K), were formed by treatments in oxidizing conditions, and were insensitive to leaching treatment. Computer simulation of the spectra yielded the following spin-Hamiltonian parameters for isolated species: $g_\parallel = 1.960$, $g_\perp = 1.843$, $A_\parallel = 34$ G, and $A_\perp = 90$ G for Mo^V_{tetr}; $g_{xx} = 1.803$, $g_{yy} = 1.883$, $g_{zz} = 1.965$, $A_{xx} = 81$ G, $A_{yy} = 61$ G, and $A_{zz} = 16$ G for Mo^V_{mon}. The ground state, spin polarization factor, and spin–orbit reduction factor were calculated by the equations of McGarvey. © 1998 Academic Press

INTRODUCTION

Our interest in molybdenum supported on zirconia arose from this system's importance as a catalyst for dehydrogenation and hydrodesulfuration reactions. In a previous paper we described the catalytic activity of MoO_x/ZrO_2 for the hydrogenation of propene and the EPR characterization of Mo^V surface species (1). Mo^V surface species formed by CO or H_2 reduction on ZrO_2 and on Al_2O_3 and TiO_2 (2, 3) have a square-pyramidal configuration, like that of the molybdenyl ion (MoO^{3-}). Because of the strong axial field along the Mo=O double bond and the consequent wide separation between the excited and the ground states, the **g** tensor is fairly close to the free-spin value and the spectrum is observed at room temperature (RT). Mo^V surface species formed on SiO_2 (3) have a tetrahedral configuration and need a temperature of 77 K for EPR detection.

Mo^V bulk species have been investigated by EPR spectroscopy in several oxide matrices (4–15). Many studies concerned oxides with a rutile structure (TiO_2, SnO_2, and GeO_2), and Mo^V ions in the substitutional or interstitial position have been found (4–11). In both positions the paramagnetic ion is in a distorted octahedral coordination, and in single-crystal and powder samples an EPR spectrum was obtained only at $T \leq 77$ K.

When Mo^V (d^1 ion) symmetry is cubic (or nearly cubic), as it is in the $SrTiO_3$ matrix (13), the orbital degeneracy of ground state T_{2g} is lifted only through the combined action of spin–orbit splitting and the dynamic Jahn–Teller effect. The **g** tensor is therefore strongly anisotropic and the EPR spectrum can be only observed at liquid-helium temperature in single crystals.

In the present paper we report a systematic study on the formation of Mo^V bulk species in zirconia and its spectroscopic properties in relation to the peculiar polymorphism of the matrix. The use of ^{95}Mo-enriched samples allowed a full analysis of the EPR spectra.

EXPERIMENTAL

Sample Preparation and Treatments

The MoO_x/ZrO_2 specimens were prepared by two methods: adsorption and coprecipitation. For adsorption the ZrO_2 support, prepared by hydrolysis of $ZrOCl_2$ with gaseous NH_3 (1) and dried at 383 K for 24 h, was shaken for 72 h at RT with a solution of ammonium heptamolybdate (AHM, Carlo Erba, RP) at pH 2. Some samples were prepared using solutions of ^{95}Mo-enriched (96.8%, Harwell, A.E.R.E.) AHM. For coprecipitation a concentrated ammonia solution ($\cong 8$ N) was added under stirring to a $ZrOCl_2$ and AHM solution. The samples were finally dried at 383 K for 24 h in air.

The MoO_x/ZrO_2 specimens are designated as ZMox(y) (Z^{95}Mox(y) for ^{95}Mo-enriched samples). The figure x gives the analytical Mo content (weight percent), determined by atomic absorption spectroscopy, and y specifies the preparation method (a, adsorption; c, coprecipitation).

The ZMo samples were treated in air or oxygen at 773 K for 5h and in air at 1073 K for 24 h. To remove the Mo fraction adsorbed on the surface without altering the location and the distribution of bulk molybdenum ions, after thermal treatment at 773 or 1073 K some samples were leached. The leaching procedure consisted of treatment with a concentrated ammonia solution ($\cong 8$N) at RT for 0.5 h,

[1] To whom correspondence should be addressed.

0022-4596/98 $25.00

treatment with a solution of 1N NaOH at 363 K for 0.5 h, thorough rinsing with distilled water, and drying at 383 K for 24 h in air. The leached ZMo samples were treated with O_2 and H_2 (Matheson, C.P.) at various temperatures in a gas circulation apparatus, as already described (1).

Characterization Techniques

After the thermal treatments in air or dry oxygen, the ZMo samples underwent X-ray diffraction analysis with a Philips PW 1729 diffractometer (Cu$K\alpha$, Ni-filtered radiation) equipped with an IBM PS2 computer (software APD-Philips).

X-band EPR spectra were recorded at RT and 77 K on a Varian E-9 spectrometer equipped with an on-line computer for data acquisition and evaluation. The magnetic field was calibrated using as a reference the sharp peak at $g = 2.0008$ of the E'1 center (16) (marked with an asterisk in Figs. 1a, 1f, and 2c); the center was formed by UV irradiation of the silica dewar used as the sample holder. Spin-Hamiltonian parameters were obtained from the calculated spectra using the program SIM14A (17). The absolute concentration of Mo^V was determined from the integrated area of the spectra, using as standards pure vanadyl compounds in the polycrystalline state, namely VO (acetylacetonate)$_2$, $VOSO_4 \cdot 5H_2O$, and VO (tetraphenylporphyrin) (16).

RESULTS AND DISCUSSION

Phase Composition

The XRD analysis of the ZMo specimens after the thermal treatments in air or dry O_2 showed the reflection lines of the tetragonal (101, $2\theta = 30.2°$) and monoclinic (111, $2\theta = 28.2°$; $11\bar{1}$, $2\theta = 31.5°$) zirconia phases (18). The phase composition of samples was calculated by the method of Toraya *et al.* (19). In samples fired at 773 K in air or dry O_2, the tetragonal phase of ZrO_2 became prevalent with increasing molybdenum content. Samples fired at 1073 K in air had an almost pure monoclinic phase and their very sharp reflection peaks indicated well-crystallized phases and large crystallites (Table 1).

Spin-Hamiltonian Parameters of Mo^V Species

In ZMo specimens fired in air or dry O_2 the EPR spectrum recorded at RT consisted of a weak axial signal ($g_\parallel = 1.953$ and $g_\perp = 1.977$), due to surface Cr^V impurity (2, 20). No Mo^V signal was recorded at RT. In contrast, the spectra recorded at 77 K showed intense and complex signals whose characteristics depended on the heating temperature and molybdenum content. In particular, in the ZMo samples fired at 1073 K, which had an almost pure monoclinic phase, the spectrum (Fig. 1a) showed a typical three-g value signal. Its spin-Hamiltonian parameters (Table 2)

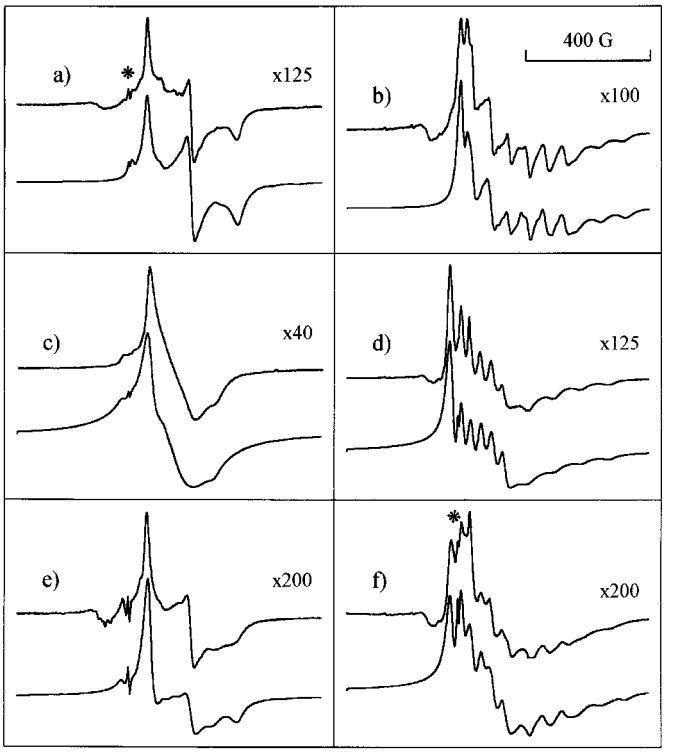

FIG. 1. ESR spectra of ZMo samples recorded at 77 K. The top traces are experimental spectra and the bottom traces are calculated spectra. The g and A parameters used for the calculation are listed in Table 2. (a) Experimental: ZMo 1.7(a), 1073 K (air); calculated: Mo^V_{mon} with Mo isotopes in natural abundance. (b) Experimental: $Z^{95}Mo$ 1.8(a), 1073 K (air); calculated: $^{95}Mo^V_{mon}$. (c) Experimental: ZMo 9.3(a), 773 K (air); calculated: Mo^V_{tetr}. (d) Experimental: $Z^{95}Mo$ 1.8(a), 773 K O_2; calculated: $^{95}Mo^V_{tetr}$. (e) Experimental: ZMo 0.7(a), 773 K (air); calculated: $Mo^V_{tetr} + Mo^V_{mon}$ (ratio 4:1). (f) Experimental: $Z^{95}Mo$ 1.8(a), 773 K (air); calculated: $^{95}Mo^V_{tetr} + {}^{95}Mo^V_{mon}$ (ratio 4:1). To obtain the best fit the spectra of samples fired at 773 K (c–f) were calculated adding Mo^V_{clust} species. The asterisk indicates the marker at $g = 2.0008$, and the figure on the experimental spectra the relative gain.

were obtained from the computer-simulated spectrum (Fig. 1a). The spectrum of the Z^{95}Mol.8(a) sample (Fig. 1b) fired at the same temperature showed well-resolved hyperfine sextets centered on g_1 and g_2, whereas the sextet centered on g_3 remained unresolved. Because the low-field region of the calculated spectrum was sensitive even to small A_3 variations, computer simulation (Fig. 1b) yielded accurate A_3 values. We assigned this signal to isolated Mo^V bulk species in the monoclinic phase (Mo^V_{mon}).

In ZMo samples containing almost exclusively the tetragonal phase of zirconia (i.e., ZMo9.3(a) fired at 773 K in air and Z^{95}Mol.8(a) fired at 773 K in dry O_2) the spectra (Figs. 1c and 1d) consisted of an axial signal, showing a well-resolved hyperfine structure in the enriched sample. Its stability to O_2 exposure at RT (see later) showed that this signal did not originate from the surface tetrahedral Mo^V

TABLE 1
Phase Composition and Concentration of Mo^V Bulk Species of MoO_x/ZrO_2 Samples after the Thermal Treatments

Sample	T^a (K)	Tetrag phase (wt%)	$[Mo^V]_{ESR}{}^b$ (%)	T^a (K)	Tetrag phase (wt%)	$[Mo^V]_{ESR}{}^b$ (%)
ZMo0.7(a)	773	27	0.013	1073	0	0.013
ZMo1.7(a)	773	55	0.027	1073	11	0.022
ZMo9.3(a)	773	100	0.050	1073	5	0.032
Z^{95}Mo0.6(a)	773	47	0.013	1073	0	0.013
Z^{95}Mo1.8(a)	773	78	0.028	1073	14	0.038
	773(O_2)	90	0.030			
ZMo5.6(c)	773 K	84	0.032	1073	0	0.025

[a] Temperature of thermal treatment in air or in dry O_2 for Z^{95}Mo1.8(a) sample.
[b] Percentage of the total molybdenum detected by ESR as Mo^V bulk species.

species, observed in the MoO_x/SiO_2 system (3). We therefore assigned this axial signal to isolated Mo^V bulk species in the tetragonal phase of ZrO_2 (Mo^Vtetr). To obtain the best fit between the computed and experimental spectra, we took into account, in addition to the axial signal, a broad ($\Delta H_{pp} = 160$ G) band with $g = 1.92$, corresponding thus to the average g value of the Mo^V_{tetr} signal (Figs. 1c and 1d). The broad signal was assigned to clustered Mo^V bulk species in the tetragonal phase (Mo^V_{clust}).

ZMo samples fired at 773 K in air containing both monoclinic and tetragonal phases yielded composite EPR spectra. In the most diluted sample (ZMo0.7(a)), which had the smallest amount of the tetragonal phase (27 wt%), the three-g-value signal of the Mo^V_{mon} species predominated, but the shoulder at $g = 1.843$ ($g_\parallel$ component of the axial signal) indicated the presence of the Mo^V_{tetr} species (Fig. 1e). In the ZMol.7(a) and ZMo5.6(c) samples, which had a larger amount of the tetragonal phase (55 and 84 wt%, respectively), the $g_\parallel$ component of the axial signal became more evident (spectra not reported). In the Z^{95}Mo spectra the presence of signals from both Mo^V species made the superimposed hyperfine patterns less resolved than those in previous spectra of enriched samples (Fig. 1f). The spectra of these ZMo samples fired at 773 K were calculated taking into account the contemporary presence of Mo^V_{mon}, Mo^V_{tetr}, and Mo^V_{clust} species (Figs. 1e and 1f).

Leaching did not affect the spectra nor did it change the relative intensity of the signals (see later), thus confirming the assignments to Mo^V species in the bulk of zirconia.

TABLE 2
Spin-Hamiltonian and Best-Fit Parameters of Mo^V Species on MoO_x/ZrO_2 Samples

Parameter	Mo^V_{tetr}	Mo^V_{mon}	Mo^V_{surf}
g_{xx}	1.960	1.803	1.955
g_{yy}	1.960	1.883	1.955
g_{zz}	1.843	1.965	1.882
A_{xx} (G)	34	81	42
A_{yy} (G)	34	61	42
A_{zz} (G)	90	16	98
g_{iso}	1.921	1.884	1.931
A_{iso} (G)	51.9	51.7	60.2
a	0	0.989	0
b	1.000	0.147	1.000
a^2/b^2	0	45/1	0
K	0.925	0.840	1.019
10^4P (cm^{-1})	−46.3	−47.5	−49.7
$\langle r^{-3}\rangle$ (au)	3.94	4.04	4.25
$P/P_0{}^a$	0.69	0.71	0.74
λ (cm^{-1})^b	712	730	764

[a] $P_0 = -69.4 \times 10^{-4}$ cm^{-1} (28).
[b] $\lambda = \lambda_0 \times (P/P_0)$, where $\lambda_0 = 1030\,cm^{-1}$ (29).

Concentration of Mo^V Species

In all ZMo specimens the total concentration of Mo^V bulk species did not depend on the method of preparation or the temperature of treatments in air or O_2 and only slightly depended on the Mo content, varying from 0.013% of the Mo content in the most diluted samples to 0.025–0.050% in the most concentrated (Table 1). The clustered Mo^V bulk species present in all the samples treated at 773 K increased in parallel with the Mo content: in the EPR spectra of more concentrated samples the broad band predominated. The presence of clustered species indicated that in the samples fired at 773 K Mo in solid solution had a nonhomogeneous distribution and possibly a concentration gradient from the surface to the interior of the ZrO_2 crystallites. Conversely, in the samples fired at 1073 K the absence of the broad band indicated that molybdenum had a random distribution.

The leaching treatment showed that, irrespective of the preparation method and the heating temperature, about 20% of the total Mo content entered in solid solution (ss) (compare columns 5 and 3 in Table 3). Whereas in accordance with our previous study all the Mo surface species were in oxidation state VI (1), some of the Mo bulk species were present as Mo^V. In particular, in the ZMol.7(a) and ZMo5.6(c) samples about 5% of the Mo present in ss is detected by EPR as Mo^V (compare columns 6 and 5 in Table 3).

To investigate the oxidation state of molybdenum ions in the zirconia matrix, ZMo5.6(c) fired in air at 773 K and leached (Mo content 0.97 wt%) was submitted to redox treatments. After reduction with H_2 at 773 K for 3 h, the spectrum at RT consisted of an intense axial signal (30% of Mo content) (Fig. 2a). We assigned this signal to Mo^V surface species (Mo^V_{surf}) in a square-pyramidal configuration (1, 2), and its g and A values are listed in Table 2. At 77 K this signal dominated the spectrum and Mo^V bulk species were

TABLE 3
Mo Content and Concentration of Mo^V Bulk Species in MoO_x/ZrO_2 Samples Submitted to Leaching Treatment

		Before leaching[a]		After leaching[a]	
Sample	T^b (K)	Mo content (wt %)	$[Mo^V]_{ESR}{}^c$ (%)	Mo content (wt%)	$[Mo^V]_{ESR}{}^c$ (%)
ZMo1.7(a)	1073	1.7	0.022	0.40	0.023
ZMo5.6(c)	773	5.6	0.032	0.97	0.045

[a] The leaching procedure consisted of (i) treatment with a solution of NH_3 (8 N) at room temperature for 0.5 h, (ii) treatment with 1 N NaOH at 363 K for 0.5 h, (iii) rinsing with distilled water, and (iv) drying at 393 K for 24 h.

[b] Temperature of the treatment in air.

[c] Percentage of the total molybdenum detected by ESR as Mo^V bulk species.

barely detectable. After exposure to O_2 at RT the superoxide species (O_2^-: $g_1 = 2.029$, $g_2 = 2.009$, and $g_3 = 2.002$) (1) yielded a strong signal and the intensity of the Mo^V_{surf} signals fell to about 10% of the Mo content (Fig. 2b). A further treatment with O_2 at 573 K destroyed the O_2^- signal and the intensity of the Mo^V_{surf} species dropped to 0.8% (Fig. 2c). The spectrum recorded at 77 K (Fig. 2d) originated entirely from Mo^V bulk species and its integrated intensity corresponded to about 16% of the total Mo content (about three times higher than that of the untreated sample). H_2 treatment at 1073 K gave similar results. We detected no signals of Mo^{III} species, observed in MoO_x/TiO_2 systems treated in the same way (11). The redox experiments indicated that the majority of molybdenum ions in ss were probably in an oxidation state other than five, for example Mo^{VI} and/or Mo^{IV} (a d^2 ion detectable only at liquid-helium temperature in single crystals). H_2 treatments increased

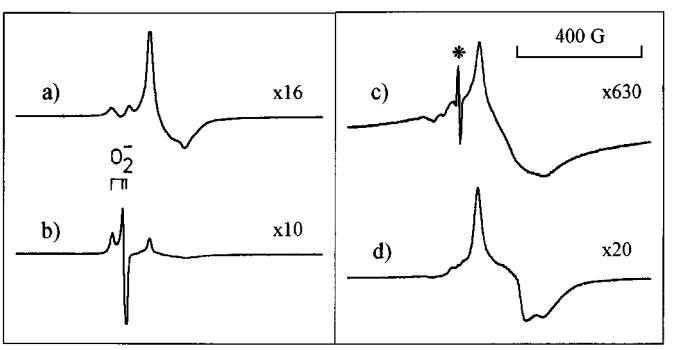

FIG. 2. ESR spectra of ZMo5.6(c), 773 K (air) after leaching treatment: (a) sample treated at 773 K in H_2, recorded at RT; (b) after O_2 adsorption and evacuation at RT, recorded at RT; (c, d) after O_2 treatment at 573 K and evacuation at RT, recorded at RT and 77 K, respectively. The asterisk indicates the marker at $g = 2.0008$, and the figure on the spectra the relative gain.

Mo^V_{bulk} concentration possibly because they reduced Mo^{VI} ions in ss.

In leached samples the formation by reduction of a strong signal of Mo^V_{surf} indicated either that the leaching treatment used did not suffice to remove all the Mo present on the surface or that some Mo near the surface, not removed by the leaching treatment, reemerged from the bulk during the redox treatments at 773 K. To clarify this point we leached the ZMo5.6(c) sample more efficiently by increasing the contact time (overnight) and repeating the treatments with NH_3 and NaOH three times. These additional procedures, however, left the Mo content practically unchanged (0.94 vs 0.97 wt%), indicating that some Mo near the surface reemerged. By removing surface Mo by leaching, the strong Mo concentration gradient between the surface itself and the nearby layers represents the driving force responsible for Mo segregation.

Symmetry and Energy Levels of the Mo^V Species

The determination of the EPR parameters of a paramagnetic species is useful to obtain detailed information on its structure and energy levels. A powder spectrum yields only the principal values of the **g** and **A** tensors, and thus a hypothesis about the location of the paramagnetic species is required. The Mo^V species showing hyperfine structure can be assumed as isolated ions in the substitutional sites (Zr^{IV}) of the tetragonal (Mo^V_{tetr}) and monoclinic (Mo^V_{mon}) phases of ZrO_2. The site symmetry is then deduced from the known crystal structure of these phases. In the tetragonal zirconia phase the cationic site has an eightfold coordination: each Zr atom is surrounded by eight oxygen atoms, four in a flattened tetrahedron and four in an elongated tetrahedron that is rotated 90° relative to the flattened one (21). Its D_{2d} symmetry yields an axial site and the z axis corresponds to the **c** axis of the tetragonal cell, thus confirming the axial EPR spectrum of the isolated Mo^V_{tetr} species.

The monoclinic phase is more complex. In a completely anisotropic spectrum (three g values) each g and A value has to be assigned to an x, y, or z component only on a theoretical basis. The consensus is that when an anisotropic spectrum of this type can be satisfactorily reproduced by computer simulation, the principal axes of the **g** and **A** tensors coincide (rhombic spectrum) (22–24). The site symmetry can then be assumed at least approximately as C_{2v}, and the z axis of the **g** and **A** tensors (g_{zz} and A_{zz} principal values) as coincident with the C_2 axis. In the monoclinic zirconia phase the cationic site has a sevenfold coordination. The ZrO_7 coordination polyhedron is irregular: all of its angles and interatomic distances differ (25), with no symmetry elements (C_1 point group). However, four oxygen atoms (the O_{II} atoms) form a planar square group (slightly distorted square array), lying in a plane parallel to (100), and

three oxygen atoms (the O_I atoms) form a triangle whose plane is nearly parallel to the plane of the O_{II} atoms. To approximate the site symmetry to C_{2v}, the most plausible choice is to take the direction perpendicular to the plane (100) as the z axis of the **g** and **A** tensors. This direction practically coincides with the **a** axis; it is tilted only by $9°14'(\beta - \pi/2)$ from it.

These hypotheses about the site symmetry and the spin-Hamiltonian parameters (Table 2) suggested the ground state and the energy levels of the Mo^V species in ZrO_2. The equations reported in Table 4 were derived from the second-order perturbation theory of McGarvey (26) and have been used by various investigators (22, 23, 27) for V^{IV} complexes of the type $[VL_2M_2]$ (L and M are organic or inorganic ligands, or both) in which the C_{2v} symmetry has been assumed. The three unknowns, a, K, and P (and then $\langle r^{-3}\rangle$), can be obtained from A_{xx}, A_{yy}, and A_{zz} and from Δg_{xx}, Δg_{yy}, and Δg_{zz}. The spin polarization factor K relates the isotropic part of the hyperfine interaction: $A_{iso} = (A_{xx} + A_{yy} + A_{zz})/3 = (-K + \Delta g_{iso})P$. For $^{95}Mo^V$, the value of $P_0 = -69.4 \times 10^{-4}\,cm^{-1}$ (free ion) is deduced from $\langle r^{-3}\rangle_0 = 5.9685$ au (28). The spin–orbit constant, λ, is equal to the free-ion value ($\lambda_0 = 1030\,cm^{-1}$ (29)) times the reduction factor P/P_0 (30). This factor, indicated as the reduced spin–orbit coupling parameter (31), is due to covalency of the metal–oxygen bonds. The equations of McGarvey take only approximately into account the covalency. A more complete model, also based on the second-order perturbation theory, is given by Mabbs and Collins (32). Their equations for the **g** and **A** tensors in C_{2v} symmetry cannot be used in the present work, because the number of unknown quantities (the molecular orbital coefficients and the K and P values) is greater than the number of experimental EPR parameters.

TABLE 4
Equations Used for the Calculation of g and A Tensors in C_{2v} Symmetry[a]

$$\Delta g_{xx} := -\frac{2\lambda(\sqrt{3}a + b)^2}{\Delta E_{yz}} \qquad \Delta g_{yy} := -\frac{2\lambda(\sqrt{3}a - b)^2}{\Delta E_{xz}} \qquad \Delta g_{zz} := -\frac{8\lambda b^2}{\Delta E_{xy}}$$

$$\Delta g_{ii} := g_{ii} - g_0 \qquad g_0 := 2.0023 \qquad (i = x, y, z)$$

$$A_{xx} := P\left[-K - \frac{2}{7}(a^2 - b^2) - \frac{4\sqrt{3}}{7}ab\left(1 + \frac{\Delta g_{zz}}{8b^2}\right) + \frac{\sqrt{3}}{14}\frac{(a + \sqrt{3}b)\Delta g_{yy}}{(\sqrt{3}a - b)} + \Delta g_{xx}\right]$$

$$A_{yy} := P\left[-K - \frac{2}{7}(a^2 - b^2) + \frac{4\sqrt{3}}{7}ab\left(1 + \frac{\Delta g_{zz}}{8b^2}\right) + \frac{\sqrt{3}}{14}\frac{(a - \sqrt{3}b)\Delta g_{xx}}{(\sqrt{3}a + b)} + \Delta g_{yy}\right]$$

$$A_{zz} := P\left[-K + \frac{4}{7}(a^2 - b^2) - \frac{\sqrt{3}}{14}\frac{(a - \sqrt{3}b)\Delta g_{xx}}{(\sqrt{3}a + b)} - \frac{\sqrt{3}}{14}\frac{(a + \sqrt{3}b)\Delta g_{yy}}{(\sqrt{3}a - b)} + \Delta g_{zz}\right]$$

[a] Ground state: $|\psi\rangle_0 = a|d_{z^2}\rangle + b|d_{x^2-y^2}\rangle$ $(a^2 + b^2 = 1)$. $P = g_0 g_n \beta\beta_n \langle r^{-3}\rangle$; ΔE_{xy}, ΔE_{xz}, and ΔE_{yz} are the energies, with respect to the ground state, of the excited states d_{xy}, d_{xz}, and d_{yz}, respectively.

In tetrahedral (or eightfold) coordination the ^2D term of the free ion is split into $^2T_2$ and ^2E terms, the second term being lower. A tetragonal distortion removes the orbital degeneracy of the E term and depending on the sign of the tetragonal splitting, the ground term is A_1 ($a = 1, b = 0$) or B_1 ($b = 1, a = 0$). In the Mo^V_{tetr} species (axial spectrum), because $|\Delta g_\parallel| > |\Delta g_\perp|$, the ground state is B_1 ($d_{x^2-y^2}$) and $b = 1$.

Mo^V_{mon} is more complex because, as said before, the assignment of the principal values of the **g** and **A** tensors to the x, y, or z axes is not known a priori. Using the equations in Table 4, we did all the possible permutations of the axes: the results indicate that the selection of the z axis is crucial for obtaining acceptable values of K and P. Indeed, taking g_1 or g_2 as the g_{zz} component yields no solution or unacceptable values for P (much higher than P_0) and K (much lower or higher than 1). The values reported in Table 2 are obtained taking g_3 as the g_{zz} component ($g_3 = g_{zz} = 1.965$); interchanging x and y only changes the sign of b respect to a (they become opposite), whereas the change in the sign of all the A_i components is immaterial. In C_{2v} symmetry the ground term is A_1 and the orbital contribution to this term is $|\Psi\rangle_0 = a|d_{z^2}\rangle + b|d_{x^2-y^2}\rangle$, where $a^2 + b^2 = 1$.

The values of a, b, K, P, and $\langle r^{-3}\rangle$, calculated from the equations in Table 4, are listed in Table 2.

Contrary to expectations the a and b coefficients in the Mo^V_{tetr} species (axial signal) and Mo^V_{mon} species markedly differred. These coefficients indicate that the Mo^V_{tetr} species has the orbital B_1 ($d_{x^2-y^2}$) as the ground state ($b = 1$) whereas the Mo^V_{mon} species has A_1 as the ground state, largely composed of d_{z^2}, with a small amount of $d_{x^2-y^2}$ character ($a^2/b^2 = 45$). This difference originates from the labeling of the reference axes (22), and, as discussed before, we chose as z axis the **c** axis of the tetragonal cell for the Mo^V_{tetr} species and the **a** axis of the monoclinic cell for Mo^V_{mon}.

Studying the structural relations between the ZrO_2 polymorphs, Smith and Newkirk (25) concluded that the most likely correlation is the **c** axis of the tetragonal form with the **c** axis of the monoclinic structure. The transformation from monoclinic to tetragonal symmetry takes place by rotation of the triangular groups of O_I atoms accompanied by minor movements of other atoms into the more symmetrical configuration. This transformation may leave the interactions between ligands and the central ion almost unchanged. If so, the energy levels remain similar and the hyperfine tensor preserves its highest component along the **c** axis of the tetragonal cell (z axis of the axial spectrum: $g_\parallel = 1.843$; $A_\parallel = 90$ G) and the collinear **c** axis of the monoclinic cell (x axis of the rhombic spectrum: $g_{xx} = 1.803$; $A_{xx} = 81$ G). This hypothesis awaits confirmation from a single-crystal study of Mo^V-doped monoclinic ZrO_2.

The relation between the EPR parameters and the energy levels of the Mo^V_{tetr} and Mo^V_{mon} species resembles that found for the Mo^V species in the octocyanomolybdate(V) complex,

$Mo(CN)_8^{3-}$ (33–36). This eight-coordinated ion can exist in two different idealized configurations: dodecahedral and square antiprism. In the $K_4Mo(CN)_8 \cdot 2H_2O$ solid solution the molybdenum ion has a dodecahedral distorted configuration, whereas when it is pure or dissolved in various solvents (H_2O, CH_3OH, or glycerol), it has been found in a distorted square-antiprism configuration. EPR data alone yielded this conclusion, because, for $|\Delta g_\parallel| < |\Delta g_\perp|$ and $|A_\parallel| < |A_\perp|$, the ground state is A_1 (d_{z^2}) in D_{2d} symmetry, whereas the opposite situation occurs in the dodecahedral configuration, namely, B_1 ($d_{x^2-y^2}$) ground state in D_{2d}.

Whereas the configurations of the Mo^V_{tetr} species in ZrO_2 and the $Mo(CN)_8^{3-}$ complex in $K_4Mo(CN)_8 \cdot 2H_2O$ solid solution correspond perfectly (dodecahedral), the Mo^V_{mon} species and the $Mo(CN)_8^{3-}$ complex in solution correspond only if the ZrO_7 polyhedron is approximated to a very distorted square antiprism, with the z axis normal to the planar square group of the O_I atoms and to the plane of the O_{II} atoms, as done before. Therefore it highly deviates from the axial symmetry so that the C_{2v} symmetry is more appropriate for the analysis of EPR spectrum.

The EPR parameters and the related molecular terms for the Mo^V_{surf} species (Table 2) differ little from those of the Mo^V_{tetr} species. The most significant spectroscopic difference is in the detection temperatures (RT for Mo^V_{surf} and 77 K for the Mo^V_{bulk} species), due to the different relaxation times. More important are the differences in the chemical reactivity, which clearly permit its characterization. For the Mo^V_{surf}, molybdenyl species in a square-planar configuration we have to use the C_{4v} symmetry. This symmetry group has the same terms as D_{2d} and the d orbitals belong to the same terms. The strong axial field along the M=O axis (z axis) splits the cubic T_{2g} term into the E (d_{xz}, d_{yz}) and the B_2 (d_{xy}), the latter being the ground term. Thus the unpaired electron is in the d_{xy} orbital, i.e., in the equatorial plane containing four oxygen ligands. In describing these complexes, Kivelson and Lee (36) gave a detailed theory that also accounts for their covalency. Their equations for the **g** and **A** tensors, neglecting covalency effects, are

$$\Delta g_\parallel = -8\lambda/\Delta E_{x^2-y^2} \qquad \Delta g_\perp = -2\lambda/\Delta E_{xz} \qquad [1]$$

$$A_\parallel = P(-4/7 - K + \Delta g_\parallel + 6\Delta g_\perp/14)$$

$$A_\perp = P(2/7 - K + 11\Delta g_\perp/14) \qquad [2]$$

The equations in Table 4 with $b = 1$ became Eqs. [1] and [2], the only difference being the interchange of the orbital $d_{x^2-y^2}$ with d_{xy}.

The P and K parameters of Mo^V_{surf} (Table 2) gave the same values of $P_0\beta_2^*$ (where β_2^* is the coefficient of the antibonding b_{2g}^* orbital occupied by the unpaired electron) and K terms evaluated according to Kivelson and Lee (37), showing the equivalence of the treatments.

REFERENCES

1. V. Indovina, A. Cimino, D. Cordischi, S. Della Bella, S. De Rossi, G. Ferraris, D. Gazzoli, M. Occhiuzzi, and M. Valigi, *in* "New Frontiers in Catalysis" (L. Guczi, *et al*., Eds.), p. 877. Elsevier Science, Budapest, 1993.
2. D. Cordischi, V. Indovina, and M. Occhiuzzi, *Appl. Surf. Sci.* **55,** 233 (1992).
3. C. Louis and M. Che, *J. Phys. Chem.* **91,** 2875 (1987).
4. R.-T. Kyi, *Phys. Rev.* **128,** 151 (1962).
5. T.-T. Chang, *Phys. Rev. A* **136,** 1413 (1964).
6. T. Shimizu, *Phys. Lett.* **23,** 20 (1966).
7. P. Meriaudeau, M. Che, and A. J. Tench, *Chem. Phys. Lett.* **31,** 547 (1975).
8. P. De Montgolfier and Y. Boudeville, *Chem. Phys. Lett.* **37,** 97 (1976).
9. P. De Montgolfier, P. Meriaudeau, Y. Boudeville, and M. Che, *Phys. Rev. B* **14,** 1788 (1976).
10. P. Meriaudeau, *Chem. Phys. Lett.* **72,** 551 (1980).
11. D. Cordischi, D. Gazzoli, and M. Valigi, *Gazz. Chim. Ital.* **113,** 579 (1983).
12. G. H. Azarbayejani and A. L. Merlo, *Phys. Rev. A* **137,** 489 (1965).
13. B. W. Faughnan, *Phys. Rev. B* **5,** 4925 (1972).
14. K. Eftaxias, P. E. Fielding, and G. Lehmann, *Chem. Phys. Lett.* **160,** 36 (1989).
15. I. N. Geifman, A. N. Usov, and P. G. Nagornyi, *Phys. Status Solidi B* **172,** 551 K73 (1992).
16. M. Occhiuzzi, S. Tuti, D. Cordischi, R. Dragone, and V. Indovina, *J. Chem. Soc., Faraday Trans.* **92,** 4337 (1996).
17. J. P. Lozos, B. M. Hoffman, and C. G. Franz, *QCPE* **20,** 295 (1974).
18. X-Ray Powder Data File, ASTM cards (a) 17-923 for the zirconia tetragonal phase and (b) 36-420 for the zirconia monoclinic phase.
19. H. Toraya, M. Yoshimura, and S. Somiya, *Commun. Am. Ceram. Soc.* **C-119** (1984).
20. D. Cordischi, M. C. Campa, V. Indovina, and M. Occhiuzzi, *J. Chem. Soc., Faraday Trans.* **90,** 207 (1994).
21. G. Teufer, *Acta Crystallogr.* **15,** 1187 (1962).
22. J. L. Petersen and L. F. Dahl, *J. Am. Chem. Soc.* **97,** 6416 (1975).
23. A. T. Casey and J. B. Raynor, *J. Chem. Soc., Dalton Trans.* 2057 (1983).
24. R. M. Golding and W. C. Tennant, *Mol. Phys.* **25,** 1163 (1973).
25. D. K. Smith and H. W. Newkirk, *Acta Crystallogr.* **18,** 983 (1965).
26. B. R. McGarvey, *in* "Electron Spin Resonance of Metal Complexes" (Teh. F. Yen, Ed.). Plenum, New York, 1969.
27. A. G. Evans, J. C. Evans, D. J. C. Espley, P. H. Morgan, and J. Mortimer, *J. Chem. Soc., Dalton Trans.* 57 (1978).
28. D. P. Madacsi, M. Stapelbroek, R. B. Bossoli, and O. R. Gilliam, *J. Chem. Phys.* **77,** 3803 (1982).
29. A. Abragam and B. Bleaney, *in* "Electron Paramagnetic Resonance of Transition Ions," pp. 399, 474. Clarendon Press, Oxford, 1970.
30. R. Gallay, J. J. van der Klink, and J. Moser, *Phys. Rev. B* **34,** 3060 (1986).
31. J. W. Orton, *in* "Electron Paramagnetic Resonance. An Introduction to Transition Group Ions in Crystals," p. 140. Ilife Books Ltd., London, 1968.
32. F. E. Mabbs and D. Collison, *in* "Studies in Inorganic Chemistry: Electron Paramagnetic Resonance of *d* Transition Metal Compounds," Vol. 16, p. 382. Elsevier, Amsterdam, 1992.
33. J. L. Hoard and J. W. Silverton, *Inorg. Chem.* **2,** 235 (1963).
34. B. R. Garvey, *Inorg. Chem.* **5,** 476 (1966).
35. B. J. Corden, J. A. Cunningham, and R. Eisenberg, *Inorg. Chem.* **9,** 356 (1970).
36. R. A. Pribush and R. D. Archer, *Inorg. Chem.* **13,** 2557 (1974).
37. D. Kivelson and S. K. Lee, *J. Chem. Phys.* **41,** 1896 (1964).